Room temperature NO_2 gas sensing of Au-loaded tungsten oxide nanowires/porous silicon hybrid structure*

Deng-Feng Wang(王登峰), Ji-Ran Liang(梁继然), Chang-Qing Li(李昌青), Wen-Jun Yan(闫文君), and Ming Hu(胡明)†

School of Electronics and Information Engineering, Tianjin University, Tianjin 300072, *China*

(Received 28 August 2015; revised manuscript received 10 October 2015; published online 20 December 2015)

In this work, we report an enhanced nitrogen dioxide (NO_2) gas sensor based on tungsten oxide (WO_3) nanowires/porous silicon (PS) decorated with gold (Au) nanoparticles. Au-loaded WO_3 nanowires with diameters of 10 nm–25 nm and lengths of 300 nm–500 nm are fabricated by the sputtering method on a porous silicon substrate. The high-resolution transmission electron microscopy (HRTEM) micrographs show that Au nanoparticles are uniformly distributed on the surfaces of WO_3 nanowires. The effect of the Au nanoparticles on the NO_2-sensing performance of WO_3 nanowires/porous silicon is investigated over a low concentration range of 0.2 ppm–5 ppm of NO_2 at room temperature (25 °C). It is found that the 10-Å Au-loaded WO_3 nanowires/porous silicon-based sensor possesses the highest gas response characteristic. The underlying mechanism of the enhanced sensing properties of the Au-loaded WO_3 nanowires/porous silicon is also discussed.

Keywords: Au-loaded, WO_3 nanowires, hybrid structure, gas sensing

PACS: 81.07.–b, 61.46.Bc, 78.67.Sc, 07.07.Df **DOI:** 10.1088/1674-1056/25/2/028102

1. Introduction

Nitrogen dioxide (NO_2), often produced in coal, coal oil or natural gas manufacturing, is a toxic gas that harms the environment and human health even at extremely low concentrations and a sub-ppm level. When the concentration of NO_2 is higher than 20 ppm, it is dangerous to the human body and may cause death. Reliable NO_2 sensor with high sensitivity, selectivity and low energy consumption is highly demanded for environmental safety and industrial control. In recent years, one-dimensional metal oxide nanocomposites have attracted enormous attention due to their unique electronic properties, flexible structures and excellent adsorptions. Many recent studies have shown that the important sensing parameters of one-dimensional metal oxide sensors can be improved by making them composite ones (e.g., dissimilar metal oxide,[1–6] organics,[7] and other semiconductors[8–11]), which opens a new door to realize smart sensor systems based on nanostructured materials in the NO_2 gas sensing industry.[12–15]

Tungsten oxide (WO_3), a typical n-type metal oxide semiconductor with a relatively large indirect band gap of 2.8 eV exhibits promising application potentials in catalytic/photocatalytic processing, humidity and temperature sensors, biosensors and photonic crystals[16–19] in comparison with their diverse crystal types and also has unique electrochromic, optochromic and gaschromic properties. In the research of gas sensor applications, the gas sensitivity of WO_3 heavily depends on film parameters, such as composition, morphology (e.g., grain size), nanostructure and microstructure (e.g., porosity, surface-to-volume ratio).[20,21] Since one-dimensional tungsten oxides, including nanowires and nanorods, exhibit high crystallinities and large surface-to-volume ratios[22–24] compared with their bulk materials, extensive efforts have been made synthesize the tungsten oxide nanostructures and assembled ordered superstructures for detecting NO_2 gas. Porous silicon (PS), fabricated simply by electrochemical etching of silicon resulting in periodically arranged arrays of pores, has been widely used as a scaffold to synthesize nanowires and nanotubes.[25–28] It is facile to tune pore diameters and pore spacing by adjusting parameters such as the type of electrolyte, the PH, and the applied voltage. Therefore, the composites of one-dimensional nanomaterials/PS may have enhancing effects.

The functional properties of the metal oxide-based gas sensors can be improved not only by tailoring the crystal size of metal oxides but also by adding noble metal (Pt, Pd, Ag, etc.).[29–32] It was observed that the surface modification of nanocrystalline metal oxide by noble metal sensitizers reduced the operating temperatures appreciably and improved the sensing properties towards target gas species. Liu *et al.*[33] reported a shape-controlled synthesis of Pd nanocubes on WO_3 nanoplates by a solvothermal method, which presented a high and fast response at room temperature. Liu *et al.*[34] also prepared a Pt-WO_3 sensor which exhibited a fast response and recovery as well as a high sensitivity compared with the undecorated sensor. Many studies have been performed to fabri-

*Project supported by the National Natural Science Foundation of China (Grant Nos. 61274074 and 61271070) and the Key Research Program of Application Foundation and Advanced Technology of Tianjin, China (Grant No. 11JCZDJC15300).

†Corresponding author. E-mail: huming@tju.edu.cn

© 2016 Chinese Physical Society and IOP Publishing Ltd

cate metal oxide semiconductor materials and to optimize their detection capability and optimum working conditions. Also, though WO_3 and Au are investigated intensively in the literature, not many studies of their properties after mixing and subsequent annealing have been conducted. What we have done for the first time is to successfully synthesize the Au-loaded WO_3 nanowires on PS substrates.

In this paper, we report a novel synthesis of Au-loaded WO_3 nanowires/PS composite, which presents good sensitivity and selectivity. In addition, the NO_2 sensing characteristics of this composite are compared with those of unloaded WO_3 nanowires/PS. The Au-loaded WO_3 nanowires/PS composite exhibiting an enhanced NO_2 response may be attributed to the excellent dispersion of Au nanoparticles on WO_3 nanowires having a very large effective surface area, leading to highly effective spillover of molecular nitrogen dioxide through Au nanoparticles onto the WO_3 nanowires surface. More importantly, this work suggests that seeking methods to form composite structures between noble metal and WO_3 nanowires/PS is a promising strategy to improve the performance of gas-sensing.

2. Experiment

The Au-loaded WO_3 nanowires/PS composites were prepared by the following process. First, the PS substrate with large pore size (1 μm–1.5 μm) was prepared by an electrochemical etching method in a Teflon double-cell configuration, which was described in detail in our previous work.[35] Silicon substrate was designed to be 22 mm ×9 mm after cutting from a p-type (100)-orientation monocrystalline silicon wafer with a resistivity of 10 Ω·cm–15 Ω·cm. The wafer was placed in an electrolyte solution, which was composed of a 1:2 volume mixture of 40-wt% hydrofluoric acid and 99.5-wt% N,N-dimethyl formamide (DMF). The etching current density and etching time were 100 mA·cm^{-2} and 8 min, respectively.[36] Before the etching process, the Si substrate was cleaned necessarily and immersed in hydrofluoric acid to remove the oxide layer. The etching process was carried out at room temperature (RT). After etching, all PS samples were rinsed with ethanol and dried in air. In order to obtain WO_3 nanowires/PS composite, a metallic tungsten film with a thickness of 150 nm was pre-deposited on the PS substrate by DC magnetron sputtering. Subsequently, the sputtered PS substrates were placed in the hot zone of a horizontal tube furnace. After the quartz tube was pumped to a vacuum of 5×10^{-2} Torr (1 Torr = 1.33322×10^2 Pa), a mixture of argon and oxygen was introduced at rates of 80 sccm and 0.5 sccm, respectively. Then the tube furnace temperature increased gradually from room temperature to 700 °C and was maintained at this temperature for 1 h. The schematic diagram for synthesizing the WO_3 nanowires/PS composite is shown in Fig. 1. Then the furnace cooled naturally to room temperature. Next, the WO_3 nanowires/PS composites were transferred into an ion sputtering chamber. A 3-inch-diameter (1 inch = 2.54 cm) gold disc with 99.995% purity was used as a sputtering target. The specimen prepared by loading Au layers with thickness values of 10, 20, and 30 Å are referred to as "10Au-WO_3NWs/PS", "20Au-WO_3NWs/PS", and "30Au-WO_3NWs/PS", respectively. Finally, the obtained samples of Au-loaded WO_3 nanowires/porous silicon were further annealed in a muffle furnace at 400 °C for 1 h with a temperature ramp up/down of 5 °C/min in order to stabilize the WO_3 nanowires structure.

The surface morphologies of the samples were investigated by field emission scanning electron microscopy (FE-SEM, Hitachi S4800). The phase structures of unloaded and Au-loaded WO_3 nanowires were examined by x-ray diffraction (XRD, RIGAKU D/MAX 2500V/PC, Cu Kα radiation). High-resolution transmission electron microscopy (HRTEM, Tecnai G2 F20) and energy dispersive x-ray spectroscopy (EDXS) were also used to confirm the presence of Au nanoparticles on WO_3 nanowires.

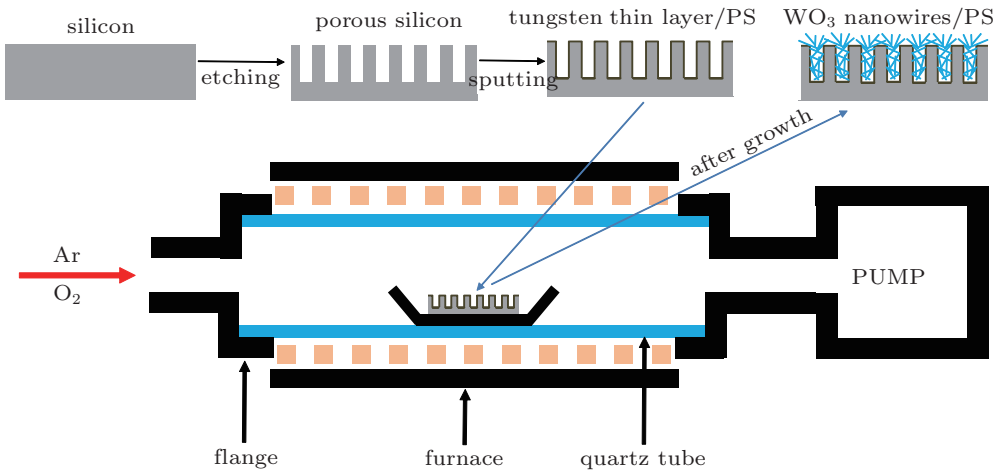


Fig. 1. (color online) Schematic diagram for synthesizing WO_3 nanowires/porous silicon composite.

The gas sensing properties of the unloaded and Au-loaded WO_3 nanowires/porous silicon were measured in a home-made testing system consisting of a sealed 30-L test chamber, a heating plate with an adjustment range of temperature from RT to 300 °C, a professional digital multimeter (NUI-T UT70D), a data acquisition PC, and a stirring mini-fan to promote the diffusion of the detected gas. Pure target gas was injected into the test chamber directly to obtain the desired concentration. The ambient relative humidity is about 35% during the entire measurement. The resistance change of the sensors during the whole measurement process was continuously monitored by the multimeter.[37] The gas sensing response (S) is given by $S = R_g/R_a$, where R_g and R_a are the resistances of the samples in oxidizing gas and air, respectively.

3. Results and discussion

3.1. Structure characterization

Figures 2(a) and 2(b) show the plain view and cross view SEM images of porous silicon with pore sizes ranging from 1.2 μm to 1.5 μm and a vertical thickness of about 14.5 μm on average. Figures 2(c) and 2(d) show the SEM images of the unloaded and Au-loaded WO_3 nanowires/porous silicon. The radial nanowires have diameters between 10 nm and 25 nm and lengths of up to 1 μm. In addition, high magnification SEM image (Fig. 1(e)) indicates that gold nanoparticles are evenly distributed on the surface of the WO_3 nanowires. As shown in Fig. 1(f), WO_3 nanowires also grow randomly inside a porous silicon structure.

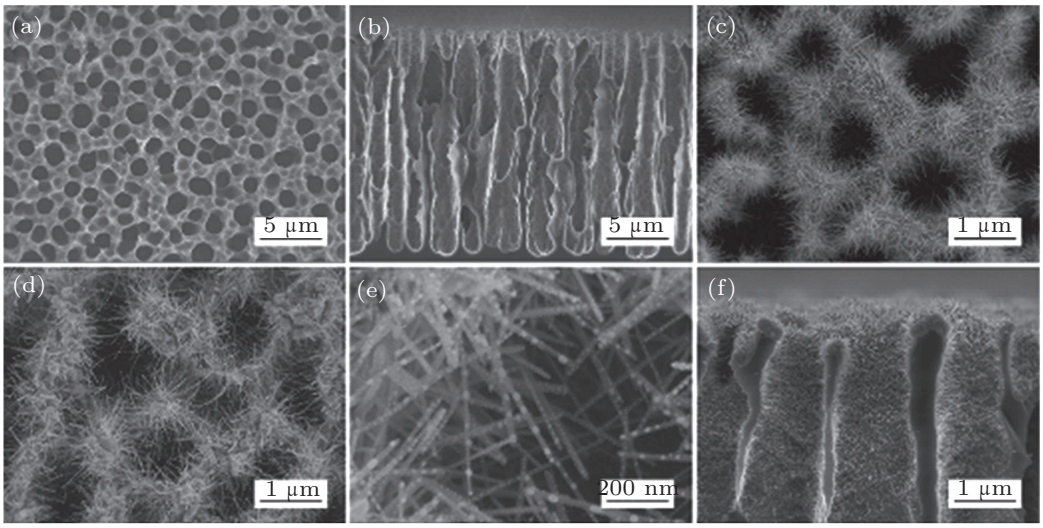


Fig. 2. SEM images of (a) plan view and (b) cross section view of the porous silicon, (c) unloaded WO_3 nanowires /porous silicon, (d) low magnification, (e) high magnification, and (f) corresponding cross-sectional SEM image of Au-loaded WO_3 nanowires.

The diffraction spectra of unloaded WO_3 nanowires and Au-loaded WO_3 nanowires with different amounts of Au content are presented in Fig. 3. The inset shows three high magnification peaks. All the diffraction peaks can be well indexed to the orthorhombic WO_3 (JCPDS 20-1324). The Au peaks can be observed at an angle of around 38.1 of 2θ (JCPDS 65-8601). Moreover, the presence of Au nanoparticles will be also proved by HRTEM and EDXS.

Figure 4(a) shows the TEM micrograph of Au-loaded WO_3 nanowires with short-axis and long-axis dimensions varying in ranges of 15 nm–20 nm and up to 1 μm, respectively. The HRTEM image (Fig. 4(b)) shows a single WO_3 nanowire with a cubic crystal structure where the lattice spacings are measured to be 0.359 nm and 0.361 nm along two orthogonal directions, respectively. Au nanoparticles, uniformly dispersed on the surfaces of WO_3 nanowires, are mostly spherical with diameters varying in a range of 1 nm–5 nm. The EDX spectrum (Fig. 4(c)) shows that the atomic concentrations of C, Cu, W, O, and Au are 33.19%, 19.02%, 12.36%, 33.34%, and 2.10%, respectively. The Cu and C elements in the EDS can be attributed to the copper grids. The XRD and SEM results indicate the successful syntheses of orthorhombic WO_3 nanowires.

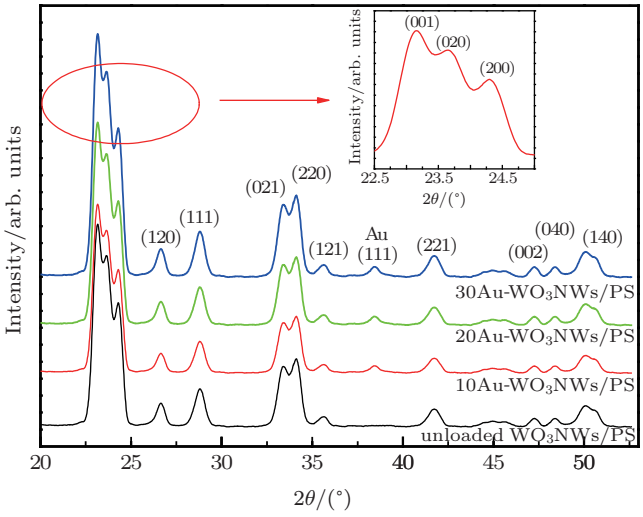


Fig. 3. (color online) XRD patterns of Au-loaded WO_3 nanowires.

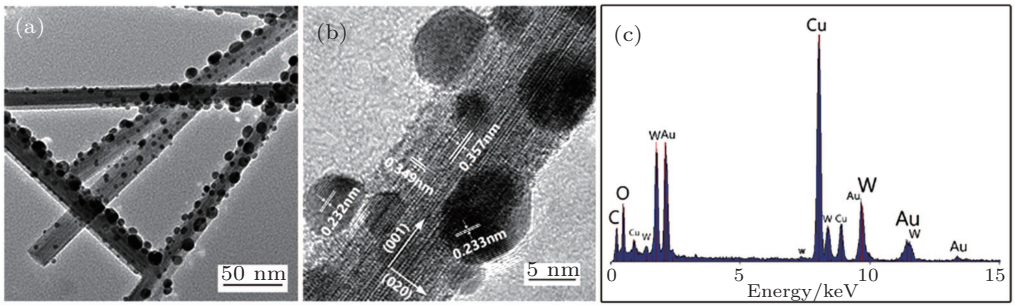


Fig. 4. (a) TEM and (b) HRTEM images and (c) EDS spectrum of obtained samples.

3.2. Gas sensing properties of NO_2

Figure 5(a) exhibits the sensing response curves of the unloaded and Au-loaded sensors for NO_2 at different concentrations at room temperature. It can be seen that the responses of these sensors vary with not only the NO_2 concentration but also the amount of Au. Besides, the 10Au-WO_3NWs/PS, which exhibits a much higher response than the unloaded WO_3NWs/PS prepared by the same method, presents the highest gas response (S) 3.357 to 2-ppm NO_2. Figure 5(b) shows the dynamic response of 10Au-WO_3NWs/PS to NO_2 gas with concentrations ranging from 0.2 ppm to 5 ppm at room temperature. Especially, the gas response to 200-ppb NO_2 is 1.331, which suggests that the sensors can be used to monitor the low concentration of NO_2 gas.

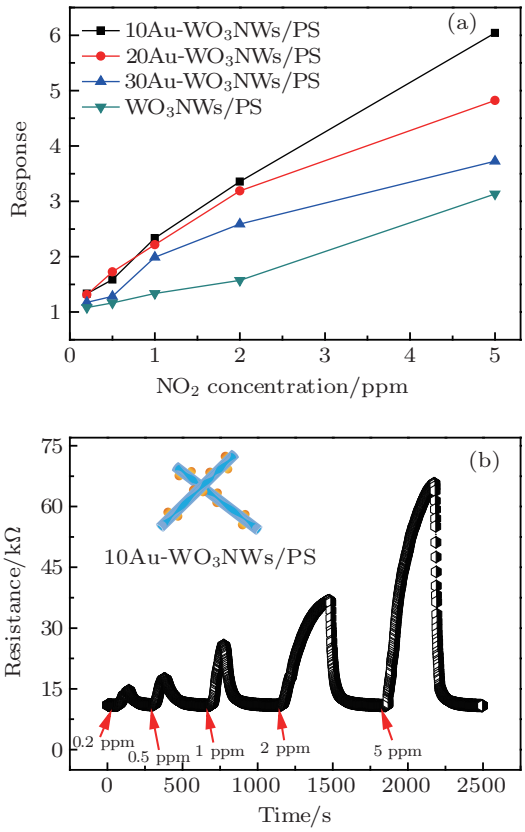


Fig. 5. (color online) (a) Sensing performances of unloaded and loaded WO_3NWs/PS to different concentrations of NO_2 at room temperature; (b) dynamic response of 10Au-WO_3NWs/PS.

3.3. NO_2 sensing mechanism

As has been reported, WO_3 is a representative n-type semiconductor with a surface-controlled sensing mechanism. The change of resistance is largely dependent on the amount and the species of chemisorbed oxygen on the surface. Figures 6(a) and 6(b) show schematic diagrams of a typical resistance change when NO_2 molecules are adsorbed and desorbed on the sensor respectively.

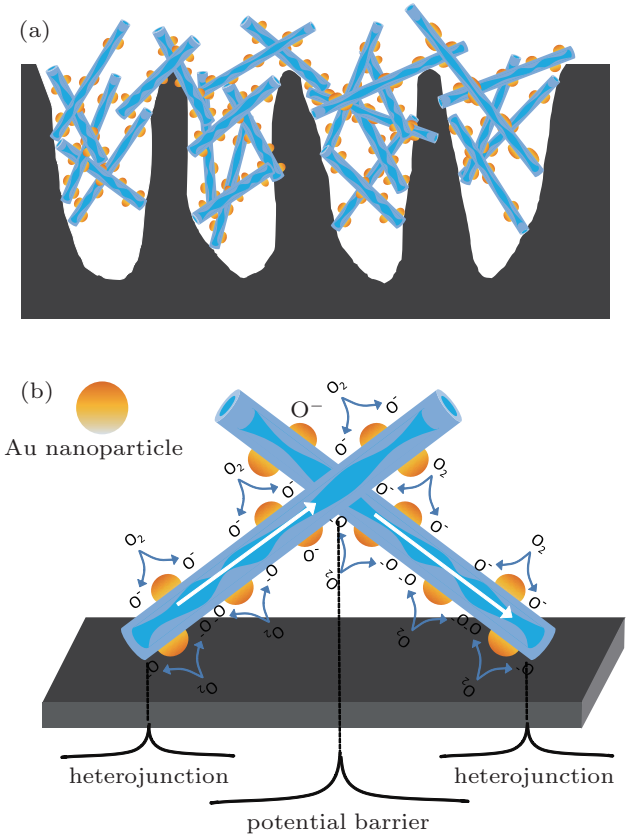


Fig. 6. (color online) (a) Schematic illustration of a network of Au-loaded WO_3 nanowires/porous silicon composite sensor and (b) the gas sensing mechanism.

The highly distributed Au nanoparticles on the surfaces of WO_3 nanowires facilitate the ion sorption of the oxygen molecules (O_2^-, O^- O^{2-}) by the well-known spillover effect through the following processes:[38–40]

$$O_2\,(\text{gas}) \rightarrow O_2\,(\text{ads}), \tag{1}$$

$$O_2\,(\text{ads}) + e^- \rightarrow O_2^-\,(\text{ads}), \quad (2)$$

$$O_2^-\,(\text{ads}) + e^- \rightarrow 2O^-\,(\text{ads}), \quad (3)$$

$$O^-\,(\text{ads}) + e^- \rightarrow O^{2-}\,(\text{ads}). \quad (4)$$

Electrons in the conduction band can be easily captured by the oxygen species. Therefore, an electron depletion layer is formed on the WO_3 nanowire surface. When NO_2 gas is introduced into the experimental cavity, it is adsorbed directly on the surface of the WO_3 nanowire and reacts with the adsorbed O^- (ads) by the following reactions:[41]

$$NO_2\,(g) + e^- \rightarrow NO_2^-\,(\text{ads}), \quad (5)$$

$$NO_2^-\,(\text{ads}) + O^-\,(\text{ads}) + 2e^- \rightarrow NO\,(g) + 2O^{2-}\,(\text{ads}). \quad (6)$$

Both reactions take free electrons from the conduction band of WO_3 resulting in a wider electron depletion layer, which is supposed to narrow the conducting channel of WO_3 nanowire thereby increasing the nanowire surface resistance. Furthermore, the heterojunction formed at the interface between WO_3 nanowire and porous silicon should also be taken into account.[42] The heterojunction prompts the electrons to flow from the porous silicon with a low work function to WO_3 with a high work function until their Fermi levels equalize, which creates an electron depletion layer or potential barrier at the interface and bends the energy band. When NO_2 gas is adsorbed, the electrons associated with these charged species are drawn from the conduction band. As a result, the initial depletion layer further extends to increase the potential barrier height of the heterojunction.

The notable phenomenon in Fig. 5(a) is that the response of the 30Au-WO_3NWs/PS sensor is low compared with the others'. It may be explained as follows: when the catalyst is added too much, under relatively high anneal temperature (400 °C), Au particles might be seriously agglomerated, which leads to the decrease of the total area of the catalyst surface. As we mentioned above, the reaction between the sensor and the gas molecules takes place on the surfaces of the additives, therefore the decrease of the total area of the catalyst surface will result in the decrease of the response. Within a certain range, the gas sensitive response decreases with the increase in gold content.

4. Selectivity

Figure 7 shows gas responses of the sensors based on 10Au-WO_3NWs/PS to 2-ppm NO_2, 50-ppm NH_3, 100-ppm ethanol, and 100-ppm acetone at 25 °C. It is clearly seen that the sensors show the highest responses to NO_2. Thus, Au-WO_3NWs/PS may be a promising sensitive material for NO_2 detection.

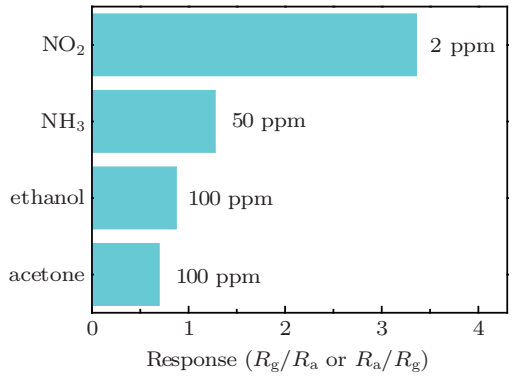


Fig. 7. (color online) Selectivities of Au-WO_3NWs/PS at room temperature.

5. Conclusions

In this work Au loaded WO_3 nanowires/PS composites with Au layer thickness values ranging from 10 Å to 30 Å, are prepared by the sputtering method. The structures and morphologies of the WO_3 nanowires are investigated by using XRD, FE-SEM, and TEM. The XRD results show that the WO_3 nanowires present a well orthorhombic system after the thermal treatment at 400 °C for 1 h. SEM and TEM analyses show that Au nanoparticles disperse evenly on the surfaces of the prepared products. The 10Au-WO_3NWs/PS sensor shows a high response (3.357) and good selectivity to 2-ppm NO_2 at room temperature. Therefore the sensor based on WO_3 with a proper Au loading demonstrates a promising process in the field of gas detection.

References

[1] Bai S L, Chen S, Zhao Y B, Guo T, Luo R X, Li D Q and Chen A F 2014 *J. Mater. Chem. A* **2** 16697
[2] Zhu C L, Chen Y J, Wang R X, Wang L J, Cao M S and Shi X L 2009 *Sens. Actuators B* **140** 185
[3] Bai S, Guo T, Zhao Y, Luo R, Li D, Chen A and Liu C C 2013 *J. Mater. Chem. A* **1** 11335
[4] Huang H, Gong H, Chow C L, Guo J, White T J, Tse M S and Tan O K 2011 *Adv. Funct. Mater.* **21** 2680
[5] Mashock M, Yu K H, Cui S M, Mao S, Lu G H and Chen J H 2012 *ACS Applied Materials & Interfaces* **4** 4192
[6] Park S, An S, Mun Y and Lee C 2013 *ACS Applied Materials & Interfaces* **5** 4285
[7] Kim I D, Rothschild A, Lee B H, Kim D Y, Jo S M and Tuller H L 2006 *Nano Lett.* **6** 2009
[8] Wongchoosuk C, Wisitsoraat A, Phokharatkul D, Tuantranont A and Kerdcharoen T 2010 *Sensors* **10** 7705
[9] Yan D L, Hu M, Li S Y, Liang J R, Wu Y Q and Ma S Y 2014 *Electrochim. Acta* **115** 297
[10] An X Q, Yu J C, Wang Y, Hu Y M, Yu X L and Zhang G J 2012 *J. Mater. Chem.* **22** 8525
[11] Niu F, Liu J M, Tao L M, Wang W and Song W G 2013 *J. Mater. Chem. A* **1** 6130
[12] Kolmakov A and Moskovits M 2004 *Ann. Rev. Mater. Res.* **34** 151
[13] Qin Y X, Liu C Y and Liu Y 2015 *Chin. Phys. B* **24** 027304
[14] Choi K J and Jang H W 2010 *Sensors* **10** 4083
[15] Batra A K, Chilvery A K, Guggilla P, Aggarwal M and Currie J R 2014 *J. Nanosci. Nanotechnol.* **14** 2065
[16] Aguir K, Lemire C and Lollman D B B 2002 *Sens. Actuators B* **84** 1

[17] Galatsis K, Li Y X, Wlodarski W, Comini E, Sberveglieri G, Cantalini C, Santucci S and Passacantando M 2002 *Sens. Actuators B* **83** 276
[18] Liu H, Duan C, Yang C, Chen X, Shen W and Zhu Z 2015 *Mater. Sci. Eng. C* **53** 43
[19] Lin W D, Lai D S, Chen M H, Wu R J and Chen F C 2013 *Mater. Res. Bull.* **48** 3822
[20] Antonik M D, Schneider J E, Wittman E L, Snow K, Vetelino J F and Lad R J 1995 *Thin Solid Films* **256** 247
[21] Moulzolf S C, Ding S A and Lad R J 2001 *Sens. Actuators B* **77** 375
[22] Bai S, Zhang K, Luo R, Li D, Chen A and Liu C C 2012 *J. Mater. Chem.* **22** 12643
[23] Qin Y, Wang F, Shen W and Hu M 2012 *J. Alloys Compd.* **540** 21
[24] Huang R, Zhu J and Yu R 2009 *Chin. Phys. B* **18** 3024
[25] Nikfarjam A, zad A I, Razi F and Mortazavi S Z 2010 *Sens. Actuators A* **162** 24
[26] Yan W, Hu M, Wang D and Li C 2015 *Appl. Surf. Sci.* **346** 216
[27] Li J, Lei W, Zhang X, Wang B and Ba L 2004 *Solid-State Electron.* **48** 2147
[28] Wang C F, Li Q S, Hu B and Li W B 2009 *Chin. Phys. B* **18** 2610
[29] Zhu L F, She J C, Luo J Y, Deng S Z, Chen J and Xu N S 2010 *J. Phys. Chem. C* **114** 15504
[30] Hoel A, Reyes L, Saukko S, Heszler P, Lantto V and Granqvist C 2005 *Sens. Actuators B* **105** 283
[31] Wang J, Zou B, Ruan S, Zhao J, Chen Q and Wu F 2009 *Mater. Lett.* **63** 1750
[32] Yin L, Chen D, Fan B, Lu H, Wang H, Xu H, Yang D, Shao G and Zhang R 2013 *Mater. Chem. Phys.* **143** 461
[33] Liu B, Cai D, Liu Y, Wang D, Wang L, Wang Y, Li H, Li Q and Wang T 2014 *Sens. Actuators B* **193** 28
[34] Samerjai T, Tamaekong N, Liewhiran C, Wisitsoraat A, Tuantranont A and Phanichphant S 2011 *Sens. Actuators B* **157** 290
[35] Ma S, Hu M, Zeng P, Yan W and Li M 2013 *Mater. Lett.* **99** 57
[36] Sun P, Hu M, Sun F Y and Xu L J 2011 *Acta Phys. Sin.* **60** 057303 (in Chinese)
[37] Qin Y, Hu M and Zhang J 2010 *Sens. Actuators B* **150** 339
[38] Kolmakov A, Klenov D, Lilach Y, Stemmer S and Moskovits M 2005 *Nano Lett.* **5** 667
[39] Van Hieu N, Van Quang V, Hoa N D and Kim D 2011 *Appl. Phys.* 657
[40] Schierbaum K D, Weimar U, Göpel W and Kowalkowski R 1991 *Sens. Actuators, B* **3** 205
[41] Oh E, Choi H Y, Jung S H, Cho S, Kim J C, Lee K H, Kang S W, Kim J, Yun J Y and Jeong S H 2009 *Sens. Actuators B* **141** 239
[42] Chérez F, Pérez-Sánchez G, Goiz O, Zaca-Morán P, Peña-Sierra R, Morales-Acevedo A, Felipe C and Soledad-Priego M 2013 *Appl. Surf. Sci.* **275** 28